Finite fault inversion of the September 25, 1999 (Mw = 6.4) Taiwan earthquake: Implications for GPS displacements of Chi-Chi, Taiwan earthquake sequence

Wu-Cheng Chi and Douglas Dreger

Seismological Laboratory, University of California at Berkeley, CA, USA

[1] The September 25, 1999 Chi-Chi Taiwan aftershock (Mw=6.4) occurred on a down dip extension of the fault ruptured in the mainshock. Strong motion data were used to invert for the finite-source process and test for the causative fault plane. We performed a grid-search over a range of focal mechanisms and found a preferred model (strike=5°, dip=30°, slip=100°) different from teleseismic studies (strike=28±10°, dip=27±5°, slip=106±9°) but similar to the mainshock (strike=5°, dip=34°, slip=65°). The aftershock asperity has a dimension of 10 km × 10 km with a maximum slip of ~1.8 m and a static stress drop of 8 MPa. We forward-predict the GPS displacements and found up to 0.033 m of surface horizontal displacements at some GPS sites, indicating that studies of post-seismic deformation may need to account for the effects of large aftershocks. *INDEX TERMS:* 1242 Geodesy and Gravity: Seismic deformations (7205); 7215 Seismology: Earthquake parameters; 7212 Seismology: Earthquake ground motions and engineering; 7230 Seismology: Seismicity and seismotectonics; 8102 Tectonophysics: Continental contractional orogenic belts

1. Introduction

[2] Taiwan is one of the most seismically active regions in the world. Several geodynamic models have been proposed to explain the mountain-building process in this region. Among them, *Willett* [1999] has proposed that the mountain region of Taiwan is underlain by a major shallow-dipping, west-vergent detachment to the west and a steeper east-vergent backthrust to the east. Strong linear seismicity in the vicinity of the proposed detachment has been observed [*Kao and Chen*, 2000]. However, the seismicity to the east is diffusive and difficult to interpret.

[3] The 1999, Chi-Chi, Taiwan earthquake (MW=7.6) earthquake caused an 80-km-long surface rupture on a west-vergent thrust (Figure 1). *Chi et al* [2001] found that slip mainly occurred within a triangular zone bounded by the towns of Sanyi, Puli, and Chusan, and inferred that fault segmentation controlled the distribution of slip. More than six Mw 6 and greater aftershocks were recorded by a very dense strong motion network [*Lee et al.*, 1999]. Here we use the data to study the finite source rupture process for one of the largest aftershocks (23.86N, 121.01E) that occurred on 1999/9/25 at 23:52:49.5 UTC.

[4] This event was recorded by more than 200 stations, and provides a unique opportunity to study the fault geometry and the rupture process at a depth (~15 km) where seismic reflection data are currently unavailable. In particular, we hope to discriminate the causative fault plane from the auxiliary plane. There are 3 scenarios for the ruptured plane: down-dip extension of the mainshock on the detachment, backthrust above the detachment, and a basement-involved fault below the detachment (Figure 1). Although the hypocenter is located in the vicinity of the proposed major shallow east-dipping fault, previous data could not exclude the possibility of a high-angle, west-dipping conjugate fault (backthrust). If true, a backthrust will give us an important constraint on the deep crustal geometry under Taiwan. In addition, recent seismicity studies (e.g. Carena et. al., EOS 82(47), p1176, 2001) show a steep, west-dipping fault below the detachment and the aftershock might have occurred on this fault, if the aftershock focal depth is actually deeper than reported. This scenario implies that large seismic strains can be stored in the footwall of the detachment and future geodynamic studies might need to consider a deformable footwall block that can generate Mw>6 earthquakes. If the rupture was on the proposed detachment, we can delineate its attitude and slip distribution, which can be compared to the mainshock. These results will add to our knowledge about stress interactions between the mainshock and aftershocks, may be used to correct the observed deformation field for aftershock contamination, and help in the study of strong ground motion attenuation by providing source parameters of the large shock.

2. Method and Results

[5] We used strong motion data from the Central Weather Bureau of Taiwan [*Lee et al.*, 1999] to invert the representation theorem for finite source parameters by using the method of *Hartzell and Heaton* [1983]. We used a linear least-squares inversion of observed velocity seismograms to compute the spatio-temporal slip distribution. To improve inversion stability, we have applied the following additional constraints: slip-positivity, Laplacian smoothing, and moment minimization.

[6] To reduce the computational cost for the inversion, we picked 11 out of the 200 stations that have high quality waveforms and provide a good azimuthal coverage. The original 50-sec, 3-component acceleration waveforms were integrated once and filtered between 0.02 and 0.5 Hz before being re-sampled at 10 sps. Compared with the predicted

(a)

(b)
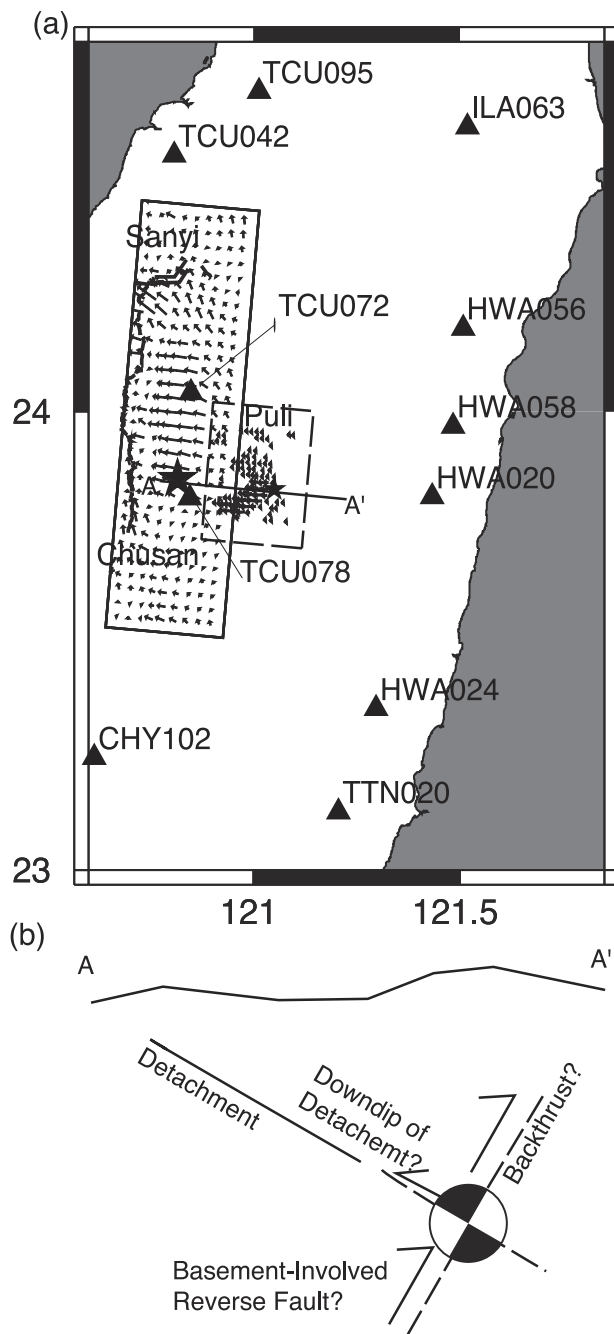
Figure 1. (a) Location map. The large star shows the epicenter of the Chi-Chi mainshock and its surface rupture is shown as the thick solid lines. The small star is the epicenter of the 9/25 event from this study. The 11 stations we used to invert the 9/25 event are plotted as triangles. The dense vectors show the 9/25 slip derived from this study. The maximum slip is 1.8 m. The sparse vectors show the mainshock model [*Chi et al.*, 2001], where the maximum slip is ~10 m. (b) A schematic cross section along AA′, showing 3 possible 9/25 rupture scenarios as discussed in the text.

arrival times from the 1D velocity model we used, we were able to pick waveforms that show no clear timing errors. Thus we used the absolute time and did not apply any time shift. We have used a square fault model with 225 subfaults
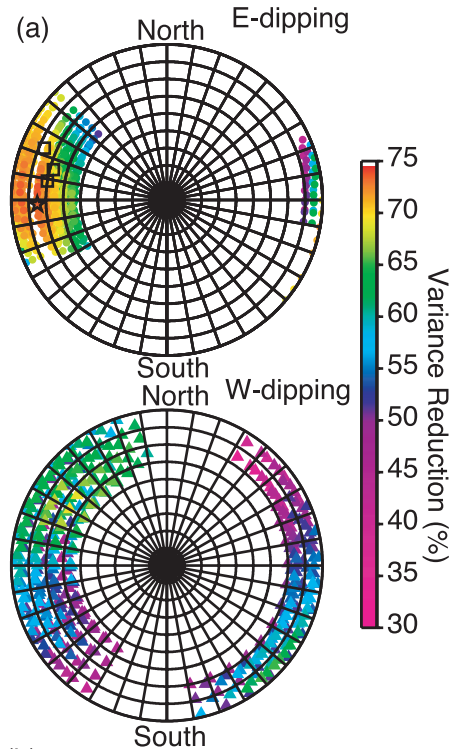
each with a dimension of 1.5 km by 1.5 km. We only allow the fault to slip in one direction (constant rake), due to the relatively smaller magnitude of this event. In this study, we use a single dislocation rise time function of 0.5 sec, consistent with *Sommerville et al.* [1999]. The time window is defined as an isosceles triangle. All subfault Green's functions are convolved with this source time history. A frequency-wave number methodology by Chandan Saikia [*Saikia*, 1994] was used to calculate a set of Green's functions based on a 1D velocity model by *Rau and Wu* [1995]. More detailed information can be found in our previous paper on the mainshock [*Chi et. al.*, 2001].

[7] For near source waveforms, the inversion is very sensitive to the focal mechanism. Therefore, we have performed a grid-search over a range of focal parameters to find the optimal orientation using the variance reduction measure (Figure 2). In total, 1036 inversions were performed. For the east-dipping plane, the ranges we have tested are strike: 0–40°; dip: 10–55°; rake: 85–125°; all with an increment of 5°; for the west-dipping plane, strike: 130–230°; dip: 30–80°; rake: 50–100°; all with an increment of 10°. The strike/dip/rake of 10°/30°/100° has the highest variance reduction of 74%. However, we chose 5°/30°/100° (variance reduction 73%) as our preferred model for its similarity to the proposed mainshock fault plane (5/34/65, *Chang et al.*, 2000). As Figure 2 shows this mechanism is allowable given the uncertainty. We then tested a range of rupture velocities and found our preferred rupture velocity to be 2.6 km/s. The waveform fits are good for the first few seconds of the pulses (Figure 3). Some higher rupture velocity runs produce a higher variance reduction (Figure 2), however, the asperity patterns become less coherent. Smaller subfaults (1 km by 1 km) were also tested and the asperity patterns are similar. The reported focal depth is 15 km and we have tested a range of focal depths with an increment of 1 km and found that depths between 11 and 17 km all give similar waveform fits (VR > 70%) but the fits deteriorate rapidly outside this depth range. We have also tested the rupture velocity on focal mechanisms derived from teleseismic data (Figure 2) and found our preferred model generally gives 10% better variance reduction.
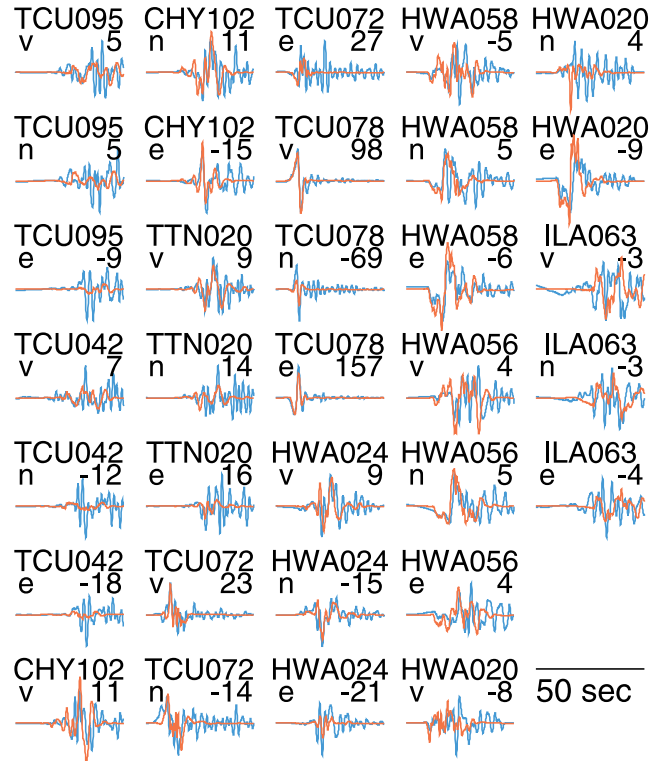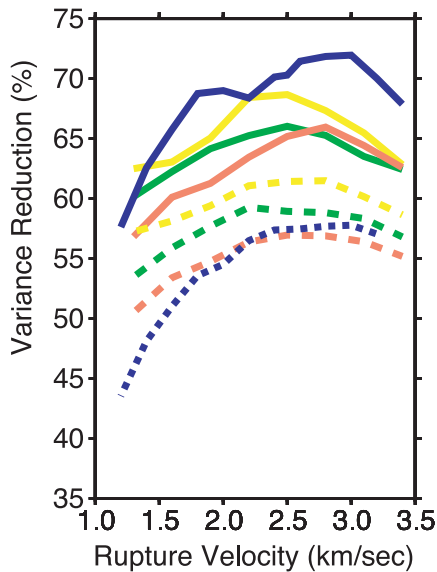
[8] All of the inversions strongly suggest that the rupture occurred on the shallow east-dipping detachment. The variance reduction for the east-dipping fault is typically 25 % higher than the conjugate, steep, west-dipping fault (Figure 2). The rupture propagates to the southwest and updip occurring within an area of 10 km × 10 km. The maximum slip is ~180 cm and the moment release 3.59e+18 N-m (Mw = 6.4). The static stress drop of the primary asperity ranges from 2.2 to 8 MPa, if we use 0 and 0.3 m as the threshold for selecting the "ruptured" subfaults, respectively.

3. Interpretation and Conclusion

[9] One surprising outcome from this study is that the strike of our preferred focal mechanism (5°) is different from that of teleseismic results (28°). An initial teleseismic moment tensor inversion for the Chi-Chi mainshock also gave a strike of 26, compared with the strike of 5° derived from the mainshock surface rupture, thus this discrepancy

Figure 3. Synthetic (red lines) and observed (blue lines) velocity waveforms. The largest amplitude for the observed waveform in mm/s is marked above each waveform. Note the large ground motion at TCU078 compared with that of HWA020.

could be systematic and relate to complex crustal velocity structures underneath Taiwan. The dip is 30° to the east. And our focal mechanism tests show that the variance reduction will drop 7% if we use a shallower dip of 10°, inferred from the reflection data collected ~10 km to the west (Wang. Chien-Ying. Unpublished data). A focal depth of 15 ± 4 km will put this aftershock on the down dip extension of the mainshock fault plane. However, it is also

(a)

(b) Rupture Velocity Sensitivity Test
Yellow: KAO (32/32/102; 198/59/83)
Green: ERI (34/25/115; 187/67/79)
Orange: CMT (18/25/102; 185/66/85)
Blue: This Study (5/30/100; 198/59/83)

Figure 2. (opposite) (a) Lower hemispheric stereonet plot showing the P axes of the focal mechanisms tested in our inversions. The color scale shows % variance reduction. The circles and the triangles are the east-dipping and west-dipping fault planes, respectively. The star shows the preferred solution (azimuth: 260; plunge: 16). The rectangles show the teleseismic focal mechanisms. The east-dipping planes give 10–20% improvements in variance reduction compared to the conjugate west-dipping planes. (b) Rupture velocity tests using different focal mechanisms. The solid-lines and dashed-lines show the results from east-dipping and west-dipping faults respectively. Overall the east-dipping faults give 10% better variance reduction than the conjugate west-dipping faults. Yellow lines are for the mechanism of *Kao and Chen* [2000], greens lines for the ERI, University of Tokyo mechanism, and orange lines are for the Harvard CMT mechanism. All of these mechanisms are derived from teleseismic data. The blue line shows the rupture velocity test using our preferred focal mechanism.

Table 1. 1D Velocity Model Used for Green's Function

Thickness km	Depth km	Vp km/s	Vs km/s	Density g/cm^3	Qp	Qs
2.2	2.2	4.5	2.6	1.8	200	100
2.2	4.4	4.85	2.8	2.05	600	300
2.2	6.6	5.3	3.06	2.25	600	300
2.2	8.8	5.6	3.23	2.39	600	300
4.5	13.3	5.84	3.37	2.5	600	300
4.5	17.8	6.13	3.54	2.64	600	300
7.5	25.3	6.28	3.63	2.7	600	300
8.5	33.8	6.6	3.81	2.85	600	300
5	38.3	6.87	3.97	2.97	600	300
21.5	60.3	7.43	4.29	3.3	600	300
25	85.3	7.8	4.5	3.3	600	300

possible that the aftershock occurred on a steeper, step-down ramp of a detachment.

[10] The aftershock's rupture extends the southern boundary of the mainshock asperity (Figure 1) which may be structurally controlled [*Chi et al.*, 2001]. For the mainshock, the slip in this region is mainly thrust with a small left-lateral component, constrained by the GPS data. On the other hand, for this aftershock, both the teleseismic and strong motion data show a thrust with a small right-lateral component. We have also tested left-lateral oblique slip in our inversion and found 10–20% decreases in variance reduction. The occurrence of this deep aftershock slip lends support that some of the poorly constrained and relatively deep mainshock slip may be real.

[11] The relatively large moment release from this aftershock indicates that its effects should be incorporated into the ongoing aftershock/afterslip studies. An excellent GPS dataset has been collected in this region [*Yu et al.*, 2001] and provides a unique opportunity to study the afterslip deformation. Depending on when the campaign GPS sites were reoccupied after the mainshock, some GPS signals might have recorded deformation from aftershocks. Our results might help recalibrate the coseismic/postseismic GPS data. Here we forward modeled the GPS displacements using our slip model in an elastic half space (c.f. *Okada*, 1992). For stations near the aftershock epicenter, most of the horizontal surface displacements are about 1/500 of the observed GPS data from the mainshock. The small displacements are due to the greater depth of this aftershock. However, the displacements can still be up to 3.3 cm at some GPS stations, and thus need to be taken into account in afterslip studies.

[12] In conclusion, the Mw = 6.4, 1999/09/25 aftershock has a focal mechanism of strike = 5°, dip = 30°, and rake = 100°, based on the strong motion data. It occurred on a shallow, east-dipping fault having a similar attitude as the mainshock fault plane. It is not on a west-dipping backthrust above the detachment nor on a west-dipping fault plane below the detachment. Rather, it images the down dip extension of the mainshock plane or possibly a ramp in a detachment. The rupture velocity is about 2.6 km/s and the slip extended the southern boundary of the asperity from the mainshock. This event has a small right-lateral component, different from the small left-lateral component of the mainshock, suggesting stress redistribution after the

mainshock or fault segmentation. We have used our slip model to forward calculate the GPS displacements and found they are relatively small compared with GPS displacements from the mainshock, however they may be large enough to be important in aftershock/afterslip studies.

References

Chi, W.-C., D. Dreger, and A. Kaverina, Finite-source modeling of the 1999 Taiwan (Chi-Chi) Earthquake derived from a dense strong-motion network, *Bull. Seism. Soc. Am.*, *91*, 1144–1157, 2001.

Chang, C.-H., Y.-M. Wu, T.-C. Chin, and C.-Y. Wang, Relocation of the 1999 Chi-Chi Earthquake in Taiwan, Terrestrial, Atmospheric and Oceanic Sciences (TAO), *11*(3), 581–590, 2000.

Hartzell, S. H., and T. H. Heaton, Inversion of strong ground motion and teleseismic waveform data for the fault rupture history of the 1979 Imperial Valley, California, Earthquake, *Bull. Seism. Soc. Am.*, *73*, 1553–1583, 1983.

Kao, H., and W.-P. Chen, The Chi-Chi earthquake sequence: active, out-of-sequence thrust faulting in Taiwan, *Science*, *288*, 346–2349, 2000.

Lee,, W. H. K., T. C. Shin, K. W. Kuo, and K. C. Chen, CWB free-field strong-motion data from the 921 Chi-Chi Earthquake: Vol. 1. digital acceleration files on CD-ROM, pre-publication Version (December 6, 1999), Seismology Center, Central Weather Bureau, Taipei, Taiwan, 1999.

Okada, Y., Internal deformation due to shear and tensile faults in a half-space, *Bull. Seism. Soc. Am.*, *82*, 1018–1040, 1992.

Rau, R.-J., and F. Wu, Tomographic imaging of lithospheric structures under Taiwan, *Earth Planet. Sci. Lett.*, *133*, 517–532, 1995.

Saikia, C. K., Modified frequency-wave-number algorithm for regional seismograms using Filon's quadrature-modeling of L(g) waves in eastern North America, *Geophys. J. Int.*, *118*, 142–158, 1994.

Sommerville, P., K. Irikura, R. Graves, S. Sawada, D. Wald, N. Abrahamson, Y. Iwasaki, T. Kagawa, N. Smith, and A. Kowada, Characterizing crustal earthquake slip models for the prediction of strong ground motion, *Seism. Res. Lett.*, *70*(1), 59–80, 1999.

Willett, S. D., Rheological dependence of extension in wedge models of convergent orogens, *Tectonophysics*, *305*(4), 419–435, 1999.

Yu, S.-B., L.-C. Kuo, Y.-J. Hsu, H.-H. Su, C.-C. Liu, C.-S. Hou, J.-F. Lee, T.-C. Lai, C.-C. Liu, C.-L. Liu, T.-F. Tseng, C.-S. Tsai, and T.-C. Shin, Preseismic deformation and coseismic displacements associated wit the 1999 Chi-Chi, Taiwan Earthquake, *Bull. Seism. Soc. Am.*, *91*, 995–1012, 2001.

W.-C. Chi and D. Dreger, Seismological Laboratory, University of California at Berkeley, Berkeley, California 94720-4767, USA. (chi@seismo.berkeley.edu; dreger@seismo.berkeley.edu)